

ZCCHC17 knockdown phenocopies Alzheimer's disease-related loss of synaptic proteins and hyperexcitability

Giuseppe P. Cortese, PhD^{1,†}, Anne Marie W. Bartosch, PhD^{2,3,†}, Harrison Xiao, ME^{2,3}, Yelizaveta Gribkova, MD^{4,5}, Tiffany G. Lam, BA^{2,3}, Elentina K. Argyrousi, PhD^{2,3}, Sharanya Sivakumar, BA^{2,3}, Christopher Cardona, BS^{2,3}, Andrew F. Teich , MD, PhD^{2,3,6,*}

¹College of Arts, Sciences, and Education, Program in Biology, Montana State University Northern, Havre, Montana, USA

²Department of Pathology and Cell Biology, Columbia University Irving Medical Center, New York, New York, USA

³Taub Institute for Research on Alzheimer's Disease and the Aging Brain, Columbia University Irving Medical Center, New York, New York, USA

⁴Department of Psychiatry, Columbia University Irving Medical Center, New York, New York, USA

⁵Division of Molecular Therapeutics, New York State Psychiatric Institute, New York, New York, USA

⁶Department of Neurology, Columbia University Irving Medical Center, New York, New York, USA

*Send correspondence to: Andrew F. Teich, MD, PhD, Department of Pathology, Columbia University, 630 West 168th Street, PH 15-124, New York, NY 10032, USA. E-mail: aft25@cumc.columbia.edu

[†]Giuseppe P. Cortese and Anne Marie W. Bartosch share joint first authorship.

ABSTRACT

ZCCHC17 is a master regulator of synaptic gene expression and has recently been shown to play a role in splicing of neuronal mRNA. We previously showed that ZCCHC17 protein declines in Alzheimer's disease (AD) brain tissue before there is significant gliosis and neuronal loss, that ZCCHC17 loss partially replicates observed splicing abnormalities in AD brain tissue, and that maintenance of ZCCHC17 levels is predicted to support cognitive resilience in AD. Here, we assessed the functional consequences of reduced ZCCHC17 expression in primary cortical neuronal cultures using siRNA knockdown. Consistent with its previously identified role in synaptic gene expression, loss of ZCCHC17 led to loss of synaptic protein expression. Patch recording of neurons shows that ZCCHC17 loss significantly disrupted the excitation/inhibition balance of neurotransmission, and favored excitatory-dominant synaptic activity as measured by an increase in spontaneous excitatory post synaptic currents and action potential firing rate, and a decrease in spontaneous inhibitory post synaptic currents. These findings are consistent with the hyperexcitable phenotype seen in AD animal models and in patients. We are the first to assess the functional consequences of ZCCHC17 knockdown in neurons and conclude that ZCCHC17 loss partially phenocopies AD-related loss of synaptic proteins and hyperexcitability.

KEYWORDS: Alzheimer's disease, Neuron hyperexcitability, sEPSC, sIPSC, Synaptic dysfunction, ZCCHC17

INTRODUCTION

Synaptic dysfunction is a critical event in Alzheimer's disease (AD) pathogenesis (1, 2), and synaptic loss correlates strongly with premortem cognitive status (3–5). These structural changes are accompanied by large-scale dysregulation of synaptic gene expression in AD brain tissue (6–8), and these findings have been replicated in recent RNA-seq studies (9–11). In animal models of AD, aberrations in synaptic physiology (12–15) and synaptic structural abnormalities (14, 16–18) have been widely reported. Several therapeutic strategies based on rescuing synaptic dysfunction are currently being pursued (19, 20), and the molecular basis for synaptic dysfunction in AD remains an outstanding question for the field.

We previously identified ZCCHC17 during a screen for master regulators of synaptic dysfunction in AD (21), and proposed ZCCHC17 as a candidate regulator that is predicted to have reduced activity in AD leading to dysregulation of gene expression across a broad range of categories, including synaptic. ZCCHC17 was discovered in 2002 while screening a cDNA library for RNA binding proteins (22) and was also independently found in 2003 using a yeast 2-hybrid screen that searched for pinin-interacting proteins (23). The exact function of ZCCHC17 is an area of active research, and recent evidence suggests that it has roles in both mRNA (24) and rRNA (25) processing, and that it may coordinate a variety of homeostatic functions in the cell (24). ZCCHC17 protein is expressed in neurons and declines in AD brain tissue before significant gliosis or neuronal loss; knockdown of ZCCHC17

in rat neuronal cultures leads to dysregulation of a wide range of genes, including synaptic genes (21). More recently, we showed that ZCCHC17 regulates neuronal RNA splicing using human iPSC-derived neurons; thus, loss of ZCCHC17 may explain a portion of splicing abnormalities in AD brain tissue (26). Further, we have shown that CNS ZCCHC17 expression predicts cognitive resilience in the setting of AD pathology (26). Support for ZCCHC17 activity may therefore represent a therapeutic strategy. All of this suggests that ZCCHC17 is integral for normal neuronal functioning. However, the proteomic and electrophysiologic consequences of ZCCHC17 knockdown have not previously been explored in neurons.

Here, we evaluated the functional consequences of reduced ZCCHC17 expression in primary cortical cultures. Consistent with ZCCHC17's predicted role as a master regulator of synaptic genes, we found that ZCCHC17 knockdown leads to a loss of synaptic protein expression using a range of markers. Patch recording of neurons showed that loss of ZCCHC17 significantly disrupts the excitation/inhibition (E/I) balance of neurotransmission and favors excitatory-dominant synaptic activity as measured by an increase in spontaneous excitatory post synaptic currents (sEPSCs) and action potential firing rate, and a decrease in spontaneous inhibitory post synaptic currents (sIPSCs). We are the first to assess the functional consequences of reduced ZCCHC17 expression in neurons, and conclude that ZCCHC17 is necessary to maintain synaptic protein expression and proper E/I balance of neurotransmission. Thus, loss of ZCCHC17 function may contribute to hyperexcitability in AD.

MATERIALS AND METHODS

Primary cortical culture

For imaging experiments, glass coverslips were coated overnight in 2% w/v poly-D-lysine hydrobromide ([PDL], Sigma P6407) in HBSS. E17 rat pup cortices were incubated in TriPLE Express (Thermo Fisher Scientific, Waltham, MA, USA, 12605036) at 37°C for 12 minutes and mechanically dissociated with repeated pipetting. Cells were plated at approximately 15 000 cells/cm² on PDL-coated coverslips in Neurobasal media (Thermo Fisher Scientific, 21103049) supplemented with B27 plus (Thermo Fisher Scientific, A3582801), Glutamax (Thermo Fisher Scientific, 35050061), and 1% penicillin/streptomycin (Thermo Fisher Scientific, 15140148). For protein collection experiments, 6-well polystyrene plates were coated with PDL solution overnight and cells were plated at approximately 125 000 cells/cm² with the supplemented neurobasal media described above. For all experiments, cells were half-fed on DIV4 and DIV7 with supplemented neurobasal media and treated on DIV7 with 1 μM of either a pool of 4 siRNA targeting ZCCHC17 (Horizon Discovery, E-105851-00-0050) or a pool of nontargeting control siRNA (Horizon Discovery, D-001910-10-50).

Immunocytochemistry

Primary antibodies used for immunocytochemistry include: anti-Postsynaptic density (PSD95) (1:500, Neuromab clone

K28/43), anti-MAP2 (1:1000, Novus, Chesterfield, MO, USA NB300213), anti-VGLUT (1:500, Synaptic Systems, Goettingen, Germany, 135302), anti-VGAT (1:500, Synaptic Systems 131011), anti-Shank3 (1:500, Synaptic Systems 162302), and anti-Gephyrin (1:500, Synaptic Systems 147011). Secondary antibodies (Invitrogen, Waltham, MA, USA) were used at a 1:1000 dilution. DIV14 rat primary cortical cultures were washed 3 times in Dulbecco's phosphate-buffered saline (DPBS) before fixing in 4% paraformaldehyde (PFA) for 20 minutes. After 2 × 5-minute washes in DPBS with 0.25% Triton-X100 and a 5-minute wash in DPBS, the cells were blocked for 1 hour in 10% goat serum in DPBS at room temperature. Cells were then stained with primary antibody prepared in 1% BSA/DPBS at 4°C overnight. After 3 × 5-minute washes in DPBS, cells were stained with secondary antibody for 1 h at room temperature. After a 5-minute wash in 4',6-diamidino-2-phenylindole (DAPI) and 2 5-minute washes in DPBS, the coverslips were mounted on slides with Vectashield (Vector Labs H-1000-10), sealed with nail polish, and stored at 4°C for later imaging.

Imaging and analysis

Confocal microscopy was used to capture Z-stack images of the cultured neurons at 63× magnification. Images were taken of the dendrites proximal to the soma, including a small section of the soma. Images were processed with CellProfiler v4.2.1 (27). Each Z-stack image was combined by a maximum intensity projection of each channel. The region of interest (ROI) for the image analysis was limited to a 50 μm length of a dendrite contiguous with the soma, with threshold held on the microtubule-associated protein 2 (MAP2) channel using the global 2-class Otsu method (28), and expanded by 2 μm in all directions. MAP2 area was measured from the 50-μm dendrite length before its expansion. To determine puncta counts, puncta were first enhanced with a 10-pixel maximum width white top hat filter, then features at a 2-pixel width or smaller were suppressed. The IdentifyPrimaryObjects module with the global robust thresholding method was used to identify immunoreactive puncta through thresholding, with a cut-off determined by the mean absolute deviation of the median after discarding 99% of the bottom intensity pixels, and 0.1% of the top intensity pixels (29). Only puncta that overlapped with the ROI were counted. Puncta count was normalized by paired MAP2 area for each image. We performed unpaired 2-sided t-test for significance.

Synaptoneurosome preparation and immunoblotting

Synaptic proteins from cultured neurons were extracted using the Syn-Per protein extraction kit according to the manufacturer's protocol (Thermo Fisher Scientific, cat #: 87793). Briefly, cultured neurons were lysed in 200 μL of Syn-Per reagent in 6-well plates and collected on ice. Samples were then centrifuged at 1200g for 10 minutes at 4°C. Supernatant was further centrifuged at 15 000g for 20 minutes at 4°C, yielding a cytosolic fraction and a synaptosomal pellet. The pellet was then lysed in 25 μL of Syn-Per reagent supplemented with protease and phosphatase inhibitors. For immunoblotting, samples were prepared under reducing conditions

in 4× Laemmli buffer, heated at 70°C for 5 minutes, and loaded onto 4%–20% Tris-Glycine Novex SDS-polyacrylamide gels (Invitrogen). Samples were then transferred onto polyvinylidene fluoride membrane (Millipore, Burlington, MA, USA), and blocked in 5% milk/phosphate-buffered saline with Tween 20 (PBS-T) for 30 minutes at room temperature. All primary antibody incubations were performed at 4°C overnight followed by 3 × 10-minute washes with PBS-T. Secondary antibody incubations were performed at room temperature for 1 hour, followed by 3 × 10-minute washes with PBS-T. The following primary antibodies (and dilutions) were used: γ -aminobutyric acid type A receptor (GABA_AR; 1:500; sc-376282; Santa Cruz Biotechnology, Dallas, TX, USA), GluA1 (1:250; 13185S; Cell Signaling), and GAPDH (1:1000; sc-47724; Santa Cruz Biotechnology) as a loading control. Horseradish peroxidase-conjugated secondary antibodies (BD Biosciences, Franklin Lakes, NJ, USA) were diluted in the range of 1:5000 (for GAPDH) to 1:7000 (for GABA_AR and GluA1 blots). Blots were then scanned using the ChemiDoc MP Imaging System (Bio-Rad, Hercules, CA, USA). Blots were stripped using Restore Western Blot Stripping Buffer (Thermo Fisher Scientific) for 15 minutes, washed 3 × 10 minutes in PBS-T, and reprobed for GAPDH as described above. Protein bands were quantified using ImageJ (NIH) and total density of each band was normalized to total protein levels for each sample as indicated by GAPDH band densities. Unpaired 2-tailed t-test was used to determine if the level of the protein of interest in the nontargeting control siRNA group differed from the level of the protein in the ZCCHC17 siRNA group. The p value listed for each protein is for an unpaired 2-tailed t-test with statistical significance of $p < 0.05$.

Electrophysiology

Passive and active membrane properties were assessed using conventional whole-cell current clamp technique as described previously (30). Briefly, primary cortical neurons were plated on 15 mm coverslips at a density of 125 000 cells per well. Cells were treated with ZCCHC17 or nontargeting control siRNA at DIV7, and recordings were performed between DIV14–16. Neuronal cultures were perfused at room temperature with an extracellular solution (145 mM NaCl, 5 mM KCl, 10 mM 4-(2-hydroxyethyl)-1-piperazineethanesulfonic acid (HEPES), 1.3 mM MgCl₂, 2 mM CaCl₂, 10 mM glucose; pH 7.3, 325 mOsm). To measure intrinsic neuronal properties and spontaneous EPSCs, neurons were held at –70 mV and recorded over 5 minutes using a MultiClamp 700B amplifier (Molecular Devices, San Jose, CA, USA) controlled with a PC running MultiClamp Commander and pClamp (Molecular Devices), and pass filtered at 2 kHz. Spontaneous IPSCs were recorded in the presence of APV and CNQX to block α -amino-3-hydroxy-5-methyl-4-isoxazolepropionic acid (AMPA) and *N*-methyl-D-aspartate (NMDA) receptors respectively (added to extracellular solution), held at 0 mV and recorded over 5 minutes as stated above. The internal solutions consisted of the following: 110 mM Cs-methanesulfonate, 10 mM Na-methanesulfonate, 10 mM EGTA, 1 mM CaCl₂, 10 mM HEPES, 10 mM TEA, 5 mM

MgATP, 0.5 mM NaGTP (pH 7.3, 305 mOsm). Pipette resistance typically registered at 5–8 m Ω . To measure action potentials, pipettes were filled with intracellular solution containing: 130 mM K-methanesulfonate, 10 mM Na-methanesulfonate, 10 mM EGTA, 1 mM CaCl₂, 10 mM HEPES, 5 mM MgATP, 0.5 mM NaGTP. Action potentials were evoked and rheobase obtained using 1 s duration depolarizing current steps that increased incrementally by 5 pA. An action potential was defined as a transient depolarization of the membrane which had a minimum rise rate >10 mV/ms and reached a peak amplitude of >0 mV. The maximum number of action potentials was measured from a 1 s current step. Quantification of action potential characteristics was carried out using custom written scripts for Igor Pro v.6 (WaveMetrics, Portland, OR, USA).

Recordings of the potassium currents were performed in whole-cell mode using a Multiclamp 700B amplifier (Molecular Devices) with a Digidata 1440A Digitizer (Molecular Devices). Signals were filtered at 1 kHz. Currents were elicited by consecutively voltage steps from –90 mV to +60 mV, and leak subtraction was performed off-line for each current. Data acquisition and off-line analysis of spontaneous EPSCs and IPSCs were performed with pClamp (Clampex version 10.4). The extracellular solution for measuring potassium currents consisted of 119 mM NaCl, 5 mM KCl, 20 mM HEPES, 30 mM glucose, 2 mM CaCl₂, 2 mM MgCl₂, and 0.001 mM glycine (330 mOsm; pH 7.3), and the intracellular solution consisted of 130 mM K-gluconate, 10 mM KCl, 5 mM HEPES, 5 mM MgCl₂, 0.06 mM CaCl₂, 0.6 mM EGTA, 2 mM MgATP, and 0.2 mM Na₂GTP (310 mOsm; pH 7.3).

Statistics

Statistical analyses were performed in GraphPad Prism using two-way ANOVA or unpaired 2-tailed t-tests, with $p < 0.05$ considered significant. sEPSC and sIPSC events were detected and analyzed with MiniAnalysis (version 6.0.3; Synaptosoft, Fort Lee, NJ, USA) as described previously (30).

RESULTS

Excitatory and inhibitory synaptic proteins are reduced with ZCCHC17 knockdown

AD is characterized by loss of synapses as well as synaptic proteins (1–5). We first determined whether common synaptic markers previously examined in AD brain tissue (31–38) are affected by ZCCHC17 knockdown. We performed immunofluorescent staining for the excitatory marker PSD95, which demonstrated loss when normalized to MAP2 (Fig. 1A, B). Interestingly, presynaptic markers of excitation (VGLUT) and inhibition (VGAT) did not show significant changes in our neuronal cultures after ZCCHC17 knockdown (Fig. 1C, D). Subsequent immunofluorescence showed that the postsynaptic excitatory marker Shank3 also did not show a significant decline after ZCCHC17 knockdown, although gephyrin did show a significant decline (Fig. 1E, F). Based on the observed decreases in excitatory and inhibitory postsynaptic scaffolding proteins, we next sought to determine whether the expression of postsynaptic receptor proteins would also change as a result of reduced ZCCHC17 levels. To test this, we prepared

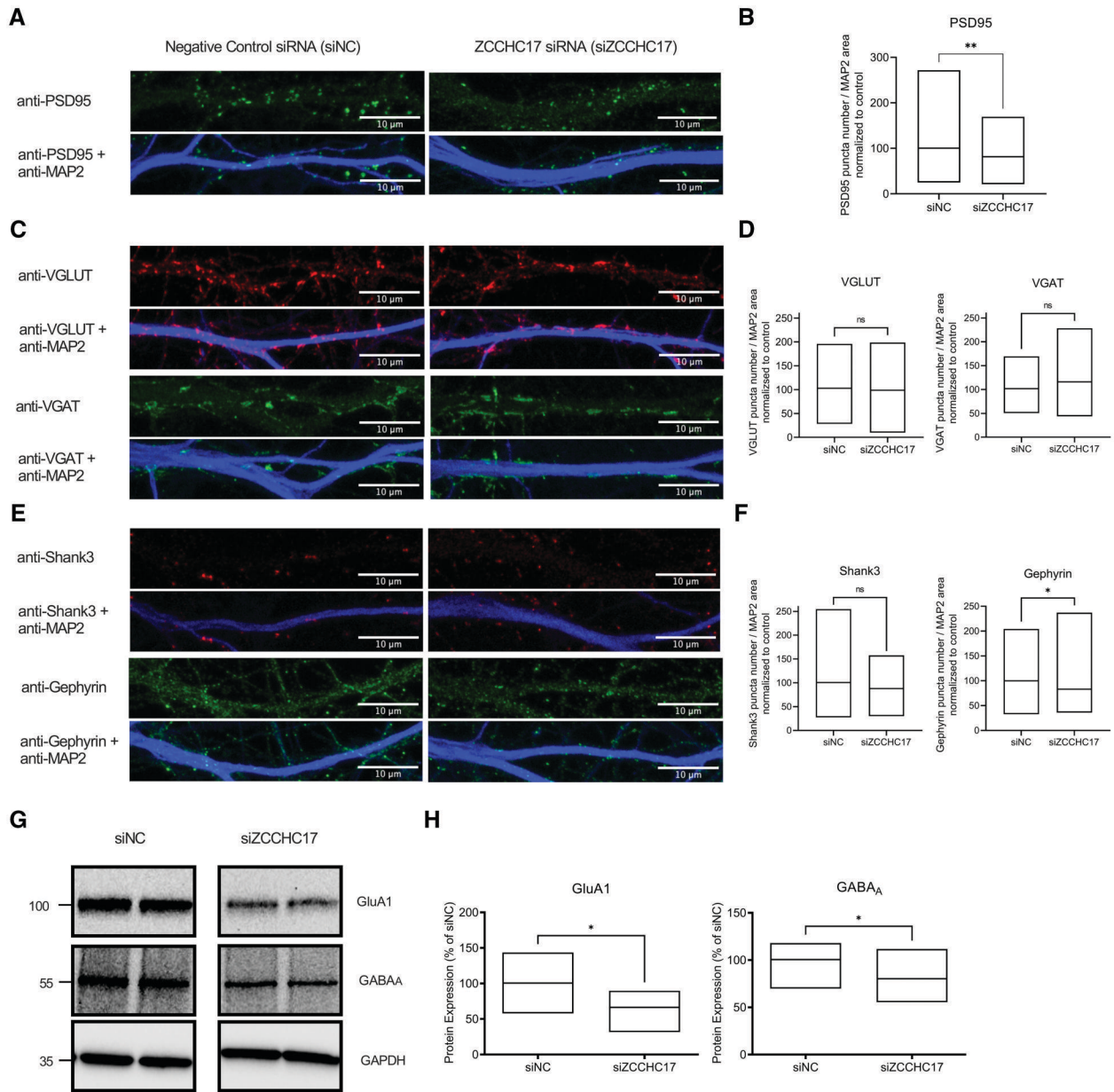


Figure 1. Levels of excitatory and inhibitory synaptic proteins are reduced with ZCCHC17 knockdown. Immunostaining in siNC or siZCCHC17 DIV14 primary cortical neurons. **(A)** Representative images of PSD95. **(B)** Quantification of PSD95 intensity normalized to the expression of neurite marker microtubule-associated protein 2 (MAP2). PSD95 is significantly decreased with ZCCHC17 knockdown ($n = 89$ and 84 for siNC and siZCCHC17, respectively; -19% ; $p = 0.0024$). **(C)** Representative images of presynaptic excitatory vesicular protein (VGLUT1) and inhibitory vesicular protein (VGAT). **(D)** Quantification of VGLUT1 ($n = 48$ and 46 for siNC and siZCCHC17, respectively, $p = 0.6773$) and VGAT ($n = 36$ and 27 for siNC and siZCCHC17, respectively, $p = 0.1567$) normalized to MAP2. **(E)** Representative images of postsynaptic excitatory protein (Shank3) and inhibitory protein (Gephyrin). **(F)** Quantification of Shank3 and Gephyrin normalized to MAP2. ZCCHC17 knockdown also produces significant decreased expression of Gephyrin ($n = 54$ for both siNC and siZCCHC17, -17% , $p = 0.034$), but not Shank3 ($n = 41$ and 38 for siNC and siZCCHC17, respectively, $p = 0.1247$). **(G)** Representative immunoblots from siNC control and siZCCHC17 samples from synaptoneurosomes prepared from DIV14 primary cortical neurons. Synaptoneurosomes were immunoblotted with antibodies against synaptic proteins: excitatory glutamate receptor (GluA1) and inhibitory GABA receptor (GABA_A). **(H)** Quantified group data for proteins expressed as a percentage of that in siNC control samples. Levels of GluA1 and GABA_A were normalized to GAPDH. $n = 9$ for each group with data from 3 independent experiments. For all graphs in figure, * denotes $p < 0.05$ using unpaired 2-tailed t-tests and data are presented with floating boxes from max to min with line at mean.

synaptic fractions (synaptoneurosomes) from primary cortical neurons treated with control and ZCCHC17 siRNA and used immunoblotting to target the postsynaptic ionotropic glutamate receptor GluA1 and the postsynaptic ionotropic GABA

receptor GABA_A. We found that synaptic levels of both the GluA1 and GABA_A receptors are significantly reduced in siZCCHC17 neurons compared to siRNA control (siNC) (Fig 1G, H).

Notably, most of the above synaptic proteins show varying levels of loss in AD brain tissue (31–36), although the evidence is weaker for VGAT (37, 38) (which also shows no change in our ZCCHC17 knockdown). In order to determine whether lower mRNA levels of these genes could at least partially explain lower levels of these proteins, we analyzed previously published RNA-seq data from Tomljanovic et al (21), in which we reported mRNA data after ZCCHC17 knockdown in the same rat cortical culture preparation used in the present paper, collected at the same timepoint as the above immunofluorescent and Western blot data. Almost all of the above synaptic proteins were significantly decreased at the mRNA level after ZCCHC17 knockdown in this dataset (Fig. 2). Shank3 is the only gene that did not decline at the mRNA level, paralleling the lack of decline at the protein level. Interestingly, the presynaptic markers VGLUT and VGAT declined at the mRNA level after ZCCHC17 knockdown, even though we find no evidence for this at the protein level by immunofluorescence. This could be due to a variety of reasons, including the fact that protein levels do not always follow mRNA levels (39); this could also be due to limitations of our immunofluorescence assay. It should also be noted that the reduction in synaptic proteins we document above could also be due to general decline in neuronal health after ZCCHC17 knockdown, in addition to any direct loss of support for synaptic gene expression. Notably, this may be particularly relevant for gephyrin, which declines at the protein level, but only nominally declines at the mRNA level, and does not pass our false discovery rate (FDR) threshold of 0.05 for multiple hypothesis correction.

Reduced ZCCHC17 expression produces neuronal hyperexcitability

Disruptions of the E/I balance of neurotransmission is known to cause neural network hyperexcitability in AD (12, 33, 40), yet few assessments have been done on the single-cell level. Here we sought to determine the neurophysiological consequences of reduced ZCCHC17 expression using whole-cell patch clamp electrophysiology recordings. Intrinsic neuronal properties and spontaneous neural activity were measured in primary cortical neurons (DIV14–16) treated with siNC control or siZCCHC17. We first determined that siRNA treatment and reduced ZCCHC17 levels have no significant effects on the intrinsic membrane properties of primary cortical neurons (Fig. 3A). Alterations in rectifier potassium channel activity occur in AD (41, 42), and contribute to hyperexcitability (43). We found that neurons with ZCCHC17 knockdown have reduced potassium current response following voltage-step stimuli (range: 0–40 mV) compared to siNC control neurons (Fig. 3B). This reduction suggests that neurons may be more prone to excitation after ZCCHC17 knockdown. To determine whether reduced ZCCHC17 expression causes intrinsic neuronal hyperexcitability, we used current-clamp methods to measure action potential frequency. We observed a significant increase in the number of action potentials in siZCCHC17 neurons compared to siNC controls (Fig. 3C, D; 20.5 ± 4.23). Next, we measured spontaneous excitatory (sEPSC) and inhibitory (sIPSC) currents in neurons expressing siNC control and siZCCHC17 to assess changes in excitatory and inhibitory neurotransmission. We observed a significant shift in the E/I ratio, as seen with an increase in the

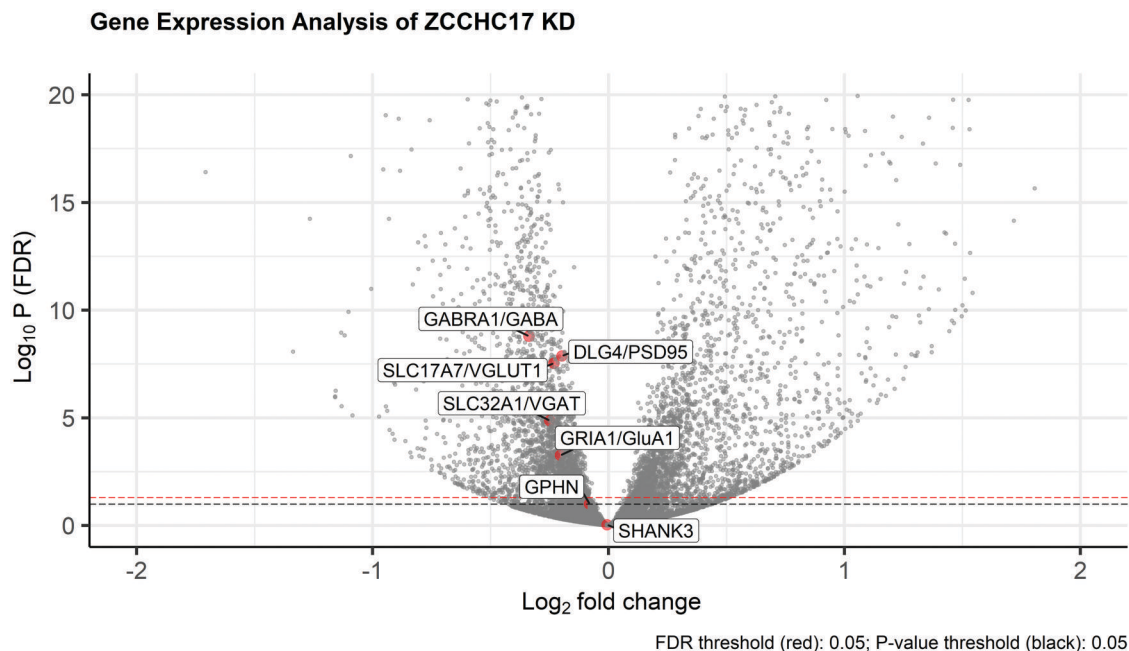


Figure 2. Differentially expressed genes in ZCCHC17 knockdown. Shown is a volcano plot for changes in gene expression after ZCCHC17 knockdown, as reported in (21) ($n = 6$ cultures with control siRNA and 6 cultures with ZCCHC17 siRNA). mRNA of proteins from Figure 1 are highlighted and labeled by both the gene and protein name. False discovery rate (FDR) p-adjusted 0.05 threshold is represented by the red dotted line and the p value 0.05 threshold is represented by the black dotted line.

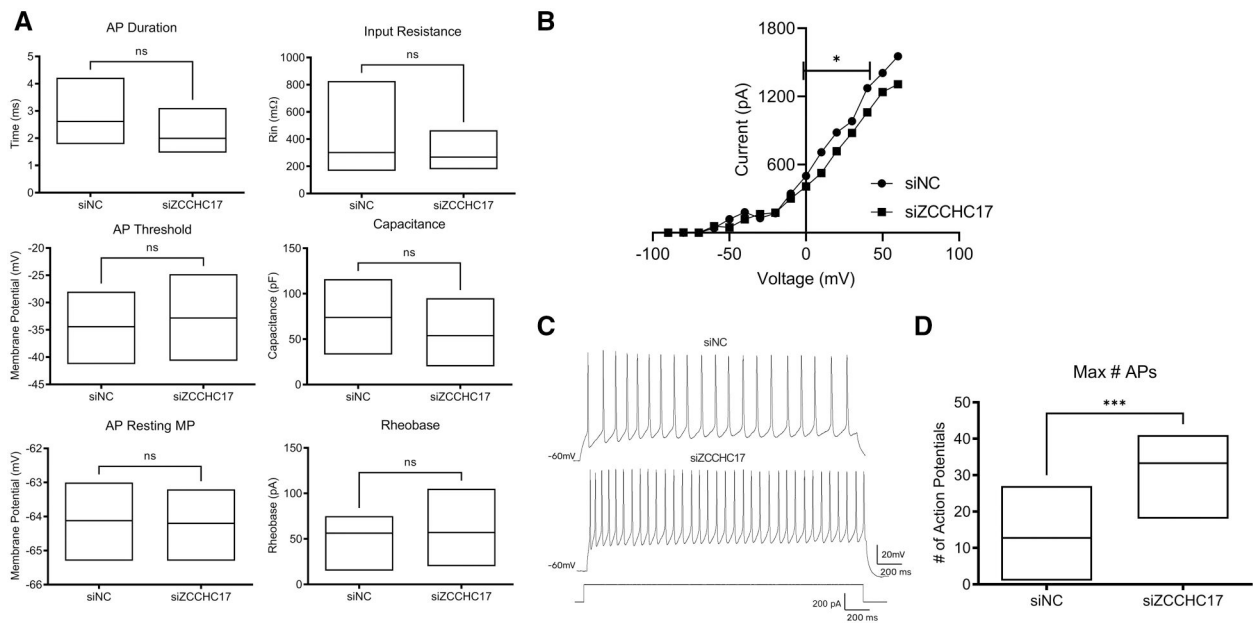


Figure 3. ZCCHC17 siRNA does not alter intrinsic neuronal properties, but increases action potential firing rate. Whole-cell patch clamp recordings from DIV14–16 primary cortical neurons treated with siZCCHC17 or siNC control. **(A)** Quantification of intrinsic membrane properties: action potential (AP) duration, AP threshold, resting membrane potential, capacitance, input resistance, and rheobase. Data presented as floating boxes from min to max with line at mean (minimum of 8 cells per group). No significant changes were detected between the 2 siRNA groups. **(B)** Potassium current (pA) in siNC and siZCCHC17 neurons following voltage steps at 10 mV increments. We observe significant reductions in potassium current following 0, 10, 20, 30, and 40 mV stimuli with ZCCHC17 knockdown (* indicates $p < 0.05$ for the current responses in the range of 0–40 mV using unpaired two-tailed t-test [0 mV: $p = 0.02$; 10 mV: $p = 0.01$; 20 mV: $p = 0.01$; 30 mV: $p = 0.01$; 40 mV: $p = 0.01$]), and there was significant overall difference between siNC and siZCCHC17 (2-way ANOVA mixed-effects model, $p = 0.01$). Asterisk indicates range of significant differences of individual currents responses between groups. $n = 20$ cells for control siRNA, 15 cells for ZCCHC17 siRNA. **(C)** Representative traces of action potentials fired in response to depolarizing current steps (1 s duration, increased incrementally by 5 pA). **(D)** Quantification of the maximum action potential presented as floating box from min to max with line at mean ($n = 8$ cells per group, $p = 0.0003$).

frequency of sEPSCs in siZCCHC17 neurons compared to siNC control neurons (Fig. 4A, B), and a decrease in sIPSC frequency (Fig. 4C, D). These findings are consistent with previous reports showing that shifts in E/I ratio produce neuronal hyperexcitability in AD (44). No significant differences were observed when comparing sEPSC (Fig. 4B) and sIPSC (Fig. 4D) amplitudes. These findings suggest that ZCCHC17 reductions disrupt the E/I balance on a single-cell level; a finding that further suggests specific targeting of glutamatergic and GABAergic activity.

DISCUSSION

It is imperative to identify key events surrounding clinical phenotypes associated with AD to develop more effective diagnostic tools and therapeutic approaches. We originally identified ZCCHC17 during a screen for master regulators of synaptic dysfunction in AD (21), and showed that ZCCHC17 protein is expressed in neurons and declines in AD brain tissue before significant gliosis or neuronal loss. Knockdown of ZCCHC17 in rat neuronal cultures led to dysregulation of a wide range of genes, including synaptic genes (21). Recently, knockdown of ZCCHC17 in human iPSC-derived neurons led to significant splicing alterations that are also altered in AD; and ZCCHC17 expression was shown to be predictive of cognitive resilience

in the setting of AD pathology (26). Given the emerging role of ZCCHC17 in neuronal dysfunction in AD, it is imperative to better understand the functional consequences of ZCCHC17 loss in neurons. Here, we begin to address this question by examining the consequences of reduced ZCCHC17 expression on synaptic protein expression and electrophysiology in primary cortical cultures. Consistent with ZCCHC17's predicted role as a master regulator of synaptic proteins, we found that loss of ZCCHC17 led to loss of synaptic protein expression using a range of markers that also decline in AD brain tissue. We also examined the electrophysiologic consequences of ZCCHC17 knockdown, and showed that loss of ZCCHC17 favors excitatory-dominant synaptic activity as measured by an increase in spontaneous EPSCs and action potential firing rate and by a decrease in spontaneous IPSCs. Thus, we conclude that ZCCHC17 is necessary to maintain proper E/I balance of neurotransmission to prevent neuronal hyperexcitability.

Hyperexcitability of neuronal networks contributes to subclinical epileptiform activity that is thought to be an early clinical feature of AD and to influence the rate of disease progression and the severity of cognitive decline (44). Human AD studies have reported periods of neuronal network hyperactivity of the hippocampus in the presymptomatic stages of familial AD (45, 46), as well as subclinical epileptiform activity

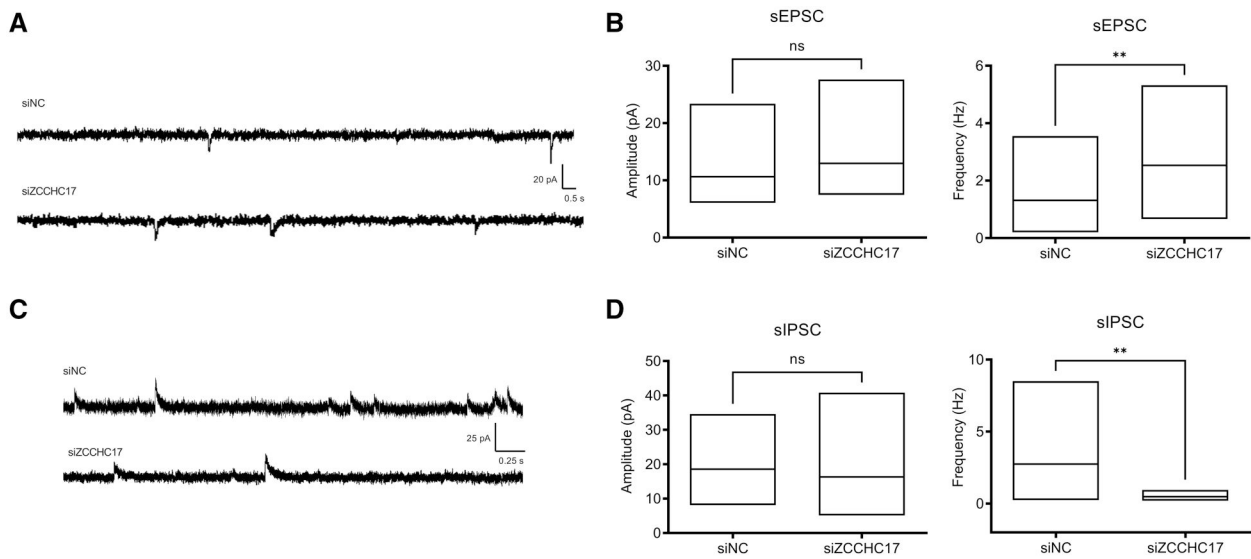


Figure 4. ZCCHC17 knockdown alters excitatory and inhibitory neurotransmission to produce hyperexcitability. Whole-cell patch clamp recordings from DIV14–16 primary cortical neurons treated with siZCCHC17 or siNC control. Spontaneous activity was recorded using voltage-clamp at -70 mV. **(A)** Representative traces of spontaneous excitatory post synaptic currents (EPSCs). **(B)** Quantification of spontaneous EPSC (sEPSC) frequency ($n = 18$ cells for siNC, $n = 15$ cells for siZCCHC17, $p = 0.009$) and amplitude ($p = 0.17$). **(C)** Representative traces of spontaneous inhibitory post synaptic currents (sIPSCs). **(D)** Quantification of sIPSC frequency ($n = 9$ cells for siNC, $n = 16$ cells for siZCCHC17, $p = 0.01$) and amplitude ($p = 0.5$). Statistical significance determined using unpaired 2-tailed t-tests and data presented as floating boxes from max to min with line at mean.

in cortical networks (47). Seizure and seizure-like activity resulting from network hyperexcitability can occur during any stage of AD, however (48, 49). Although this neurophysiological phenomenon has been observed in AD patients, the underlying neurobiological mechanisms are not fully known. The balance between excitatory and inhibitory neurotransmission, as determined by postsynaptic currents through excitatory glutamate and inhibitory GABA receptors, is necessary for normal network function (50, 51). Thus, it has been proposed that shifting of the E/I balance to favor excitatory glutamatergic neurotransmission may contribute to overall network hyperactivity in AD (33).

How a disease of synaptic loss and dysfunction produces hyperactivity is an area of active research. Although there is some evidence that excitatory neurons are preferentially affected (at least initially) by tau (52, 53), there are also alterations in inhibitory neurons in AD brain (37), and a number of studies show that hyperexcitability in AD results from reduced inhibitory (GABAergic) synaptic activity thereby creating an excitatory (glutamatergic) dominant system (54–56). This highlights the fact that both excitatory and inhibitory synapses are affected in AD and implies that any resulting hyperactivity results from an overall increase in excitation over inhibition, likely through a diversity of mechanisms. Our findings are consistent with recent work documenting this imbalance in human tissue, where an overall decline in both PSD-95 and gephyrin has been shown to still favor overall excitation both at the structural and electrophysiologic level (33). As research continues in this area, the findings in this study may provide an additional model for future work investigating one component of hyperexcitability in AD. Along these lines, it is also

important to note that our work was limited in its scope to an in vitro model of otherwise healthy neurons and that an intervention providing ZCCHC17 rescue has not yet been attempted in an AD model. We hypothesize, given the functional consequences of ZCCHC17 knockdown found in this study, that therapeutic upregulation of ZCCHC17 in an AD model would support synaptic function and could even partially rescue the hyperexcitable phenotype documented in AD brains. Future work aimed at the development of ZCCHC17-supporting agents would be valuable to further understanding its role in the context of AD pathology.

It is worth noting that frank synapse loss in human tissue specimens follows β -amyloid deposition (57), and most work shows that synapse loss is found in the context of at least mild clinical impairment (1, 3, 58–64). Some brain regions may show more resistance to synapse loss, however (65, 66). Thus, clinically apparent synaptic dysfunction in AD patients likely follows years of prodromal disease. We previously showed that ZCCHC17 loss precedes gliosis and neuronal loss, that ZCCHC17 levels predict cognitive resilience, and that ZCCHC17 dysfunction may be related to tau accumulation (21, 26). Thus, our prior work suggests that ZCCHC17 dysfunction is likely most relevant at the point of tau accumulation and cognitive decline, but before later degenerative change. Although we cannot exclude a role for ZCCHC17 dysfunction at an earlier time point, therapeutic rescue of ZCCHC17 dysfunction is probably most relevant at initial clinical presentation, rather than during the prodromal phase of AD. In light of this discussion, it bears emphasizing that ZCCHC17 dysfunction is likely a downstream consequence of AD pathology, not an initiating event in AD pathogenesis.

The exact function of ZCCHC17 is a subject of ongoing investigation. ZCCHC17 has a single zinc finger (23) and therefore is unlikely to function as a classical transcription factor. While its role in RNA splicing is increasingly appreciated (24, 26), it has also been shown to coprecipitate with a variety of other RNA binding proteins (26), and its effect on overall mRNA levels may be multifactorial. Given its wide reach as a master regulator and involvement with many RNA binding proteins, it would be beneficial to understand its druggability by determining whether ZCCHC17 rescue supports restoration of synaptic function in AD neurons and to what extent ZCCHC17 overexpression is safely tolerated in neurons. Indeed, RNA binding proteins themselves have recently been appreciated as druggable targets in a variety of diseases, although the safety profile varies depending on the specific target (67, 68). Ultimately, this is a question that cannot solely be addressed in culture systems, and will necessitate in vivo animal models. In our own work we have found that ZCCHC17 also coprecipitates with an array of proteins not related to RNA processing, including proteins involved in synaptic vesicle cycling, autophagy, and stress granule formation (26). This is consistent with observations by other laboratories that ZCCHC17 may coordinate a variety of homeostatic functions in the cell (24). While ZCCHC17's effect on synaptic gene expression is an obvious candidate for explaining its effect on synaptic proteins, there could also be degeneration secondary to declining neuronal health from a variety of other mechanisms. Thus, it will be important in future work to untangle exactly how impaired ZCCHC17 function impacts synaptic function in AD.

In summary, we have explored the synaptic and physiologic consequences of impaired ZCCHC17 function, and documented both loss of synaptic proteins and an overall increase in excitatory activity, consistent with findings from AD brain tissue. This raises the question of how ZCCHC17 is impaired in AD and how this leads to synapse failure. Recent work has shown that ZCCHC17 coprecipitates with RNA-binding proteins that also coprecipitate with tau (26). It is still unclear whether abnormal tau levels destabilize ZCCHC17 function. Future work will focus on this pathway as an avenue for tau-mediated neurodegeneration in AD.

FUNDING

AFT is supported by R03AG048077 (National Institutes of Health-National Institute on Aging), R01AG059854 (National Institutes of Health-National Institute on Aging), and NIRG-13-283742 (Alzheimer's Association). GPC is supported by P20GM103474 (National Institutes of Health-National Institute of General Medical Sciences).

ACKNOWLEDGEMENTS

The authors would like to thank Drs Clarissa Waites and Damian Williams for their advice and discussion regarding synaptic protein markers and electrophysiological protocols

and data analyses. We thank Haley Mattila for assisting with Western blotting, and Dr Ottavio Arancio for the use of his laboratory patch clamp equipment.

CONFLICT OF INTEREST

The authors declare no conflicts of interest.

REFERENCES

1. Scheff SW, Price DA, Schmitt FA, et al. Synaptic alterations in CA1 in mild Alzheimer disease and mild cognitive impairment. *Neurology* 2007;68:1501–8
2. Davies CA, Mann DM, Sumpter PQ, et al. A quantitative morphometric analysis of the neuronal and synaptic content of the frontal and temporal cortex in patients with Alzheimer's disease. *J Neurol Sci* 1987;78:151–64
3. DeKosky ST, Scheff SW. Synapse loss in frontal cortex biopsies in Alzheimer's disease: correlation with cognitive severity. *Ann Neurol* 1990;27:457–64
4. Terry RD, Masliah E, Salmon DP, et al. Physical basis of cognitive alterations in Alzheimer's disease: synapse loss is the major correlate of cognitive impairment. *Ann Neurol* 1991;30:572–80
5. de Wilde MC, Overk CR, Sijben JW, et al. Meta-analysis of synaptic pathology in Alzheimer's disease reveals selective molecular vesicular machinery vulnerability. *Alzheimers Dement* 2016;12:633–44
6. Liang WS, Dunckley T, Beach TG, et al. Altered neuronal gene expression in brain regions differentially affected by Alzheimer's disease: a reference data set. *Physiol Genomics* 2008;33:240–56
7. Liang WS, Dunckley T, Beach TG, et al. Neuronal gene expression in non-demented individuals with intermediate Alzheimer's disease neuropathology. *Neurobiol Aging* 2010;31:549–66
8. Liang WS, Dunckley T, Beach TG, et al. Gene expression profiles in anatomically and functionally distinct regions of the normal aged human brain. *Physiol Genomics* 2007;28:311–22
9. Zhou Y, Song WM, Andhey PS, et al. Human and mouse single-nucleus transcriptomics reveal TREM2-dependent and TREM2-independent cellular responses in Alzheimer's disease. *Nat Med* 2020;26:131–42
10. Mostafavi S, Gaiteri C, Sullivan SE, et al. A molecular network of the aging human brain provides insights into the pathology and cognitive decline of Alzheimer's disease. *Nat Neurosci* 2018;21:811–19
11. Huang W, Bartosch AM, Xiao H, et al. An immune response characterizes early Alzheimer's disease pathology and subjective cognitive impairment in hydrocephalus biopsies. *Nat Commun* 2021;12:5659
12. Palop JJ, Chin J, Roberson ED, et al. Aberrant excitatory neuronal activity and compensatory remodeling of inhibitory hippocampal circuits in mouse models of Alzheimer's disease. *Neuron* 2007;55:697–711
13. Trinchese F, Liu S, Battaglia F, et al. Progressive age-related development of Alzheimer-like pathology in APP/PS1 mice. *Ann Neurol* 2004;55:801–14
14. Wei W, Nguyen LN, Kessels HW, et al. Amyloid beta from axons and dendrites reduces local spine number and plasticity. *Nat Neurosci* 2010;13:190–6
15. Palop JJ, Mucke L. Epilepsy and cognitive impairments in Alzheimer disease. *Arch Neurol* 2009;66:435–40
16. Siskova Z, Justus D, Kaneko H, et al. Dendritic structural degeneration is functionally linked to cellular hyperexcitability in a mouse model of Alzheimer's disease. *Neuron* 2014;84:1023–33

17. Popugaeva E, Pchitskaya E, Bezprozvanny I. Dysregulation of neuronal calcium homeostasis in Alzheimer's disease—as therapeutic opportunity? *Biochem Biophys Res Commun* 2017;483:998–1004
18. Smith DL, Pozueta J, Gong B, et al. Reversal of long-term dendritic spine alterations in Alzheimer disease models. *Proc Natl Acad Sci U S A* 2009;106:16877–82
19. Teich AF, Arancio O. Is the amyloid hypothesis of Alzheimer's disease therapeutically relevant? *Biochem J* 2012;446:165–77
20. Chen Y, Fu AKY, Ip NY. Synaptic dysfunction in Alzheimer's disease: mechanisms and therapeutic strategies. *Pharmacol Ther* 2019;195:186–98
21. Tomljanovic Z, Patel M, Shin W, et al. ZCCHC17 is a master regulator of synaptic gene expression in Alzheimer's disease. *Bioinformatics* 2018;34:367–71
22. Gueydan C, Wauquier C, De Mees C, et al. Identification of ribosomal proteins specific to higher eukaryotic organisms. *J Biol Chem* 2002;277:45034–40
23. Chang W-L, Lee D-C, Leu S, et al. Molecular characterization of a novel nucleolar protein, pNO40. *Biochem Biophys Res Commun* 2003;307:569–77
24. Lin YM, Chu PH, Li YZ, et al. Ribosomal protein pNO40 mediates nucleolar sequestration of SR family splicing factors and its overexpression impairs mRNA metabolism. *Cell Signal* 2017;32:12–23
25. Lin YM, Chu PH, Ouyang P. Ectopically expressed pNO40 suppresses ribosomal RNA synthesis by inhibiting UBF-dependent transcription activation. *Biochem Biophys Res Commun* 2019;516:381–87
26. Bartosch AMW, Youth EHH, Hansen S, et al. ZCCHC17 Modulates neuronal rna splicing and supports cognitive resilience in Alzheimer's disease. *J Neurosci* 2024;44:e2324222023
27. Stirling DR, Swain-Bowden MJ, Lucas AM, et al. CellProfiler 4: improvements in speed, utility and usability. *BMC Bioinform* 2021;22:433
28. Otsu N. A threshold selection method from gray-level histograms. *IEEE Trans Syst Man Cybern* 1979;9:62–6
29. Falkovich R, Danielson EW, Perez de Arce K, et al. A synaptic molecular dependency network in knockdown of autism- and schizophrenia-associated genes revealed by multiplexed imaging. *Cell Rep* 2023;42:112430
30. Cortese GP, Zhu M, Williams D, et al. Parkin deficiency reduces hippocampal glutamatergic neurotransmission by impairing AMPA receptor endocytosis. *J Neurosci* 2016;36:12243–58
31. Agarwal S, Tannenbergr RK, Dodd PR. Reduced expression of the inhibitory synapse scaffolding protein gephyrin in Alzheimer's disease. *J Alzheimers Dis* 2008;14:313–21
32. Limon A, Reyes-Ruiz JM, Mileli R. Loss of functional GABA(A) receptors in the Alzheimer diseased brain. *Proc Natl Acad Sci U S A* 2012;109:10071–6
33. Lauterborn JC, Scaduto P, Cox CD, et al. Increased excitatory to inhibitory synaptic ratio in parietal cortex samples from individuals with Alzheimer's disease. *Nat Commun* 2021;12:2603
34. Wakabayashi K, Narisawa-Saito M, Iwakura Y, et al. Phenotypic down-regulation of glutamate receptor subunit GluR1 in Alzheimer's disease. *Neurobiol Aging* 1999;20:287–95
35. Gong Y, Lippa CF, Zhu J, et al. Disruption of glutamate receptors at Shank-postsynaptic platform in Alzheimer's disease. *Brain Res* 2009;1292:191–8
36. Poirel O, Mella S, Videau C, et al. Moderate decline in select synaptic markers in the prefrontal cortex (BA9) of patients with Alzheimer's disease at various cognitive stages. *Sci Rep* 2018;8:938
37. Garcia-Marin V, Blazquez-Llorca L, Rodriguez JR, et al. Diminished perisomatic GABAergic terminals on cortical neurons adjacent to amyloid plaques. *Front Neuroanat* 2009;3:28
38. Mitew S, Kirkcaldie MT, Dickson TC, et al. Altered synapses and gliotransmission in Alzheimer's disease and AD model mice. *Neurobiol Aging* 2013;34:2341–51
39. Gry M, Rimini R, Stromberg S, et al. Correlations between RNA and protein expression profiles in 23 human cell lines. *BMC Genomics* 2009;10:365
40. Verret L, Mann EO, Hang GB, et al. Inhibitory interneuron deficit links altered network activity and cognitive dysfunction in Alzheimer model. *Cell* 2012;149:708–21
41. Campolongo P, Ratano P, Ciotti MT, et al. Systemic administration of substance P recovers beta amyloid-induced cognitive deficits in rat: involvement of Kv potassium channels. *PLoS One* 2013;8:e78036
42. Pouloupoulou C, Markakis I, Davaki P, et al. Aberrant modulation of a delayed rectifier potassium channel by glutamate in Alzheimer's disease. *Neurobiol Dis* 2010;37:339–348
43. Frazzini V, Guarnieri S, Bomba M, et al. Altered Kv2.1 functioning promotes increased excitability in hippocampal neurons of an Alzheimer's disease mouse model. *Cell Death Dis* 2016;7:e2100
44. Hector A, Brouillette J. Hyperactivity induced by soluble amyloid-beta oligomers in the early stages of Alzheimer's disease. *Front Mol Neurosci* 2020;13:600084
45. Quiroz YT, Budson AE, Celone K, et al. Hippocampal hyperactivation in presymptomatic familial Alzheimer's disease. *Ann Neurol* 2010;68:865–75
46. Sepulveda-Falla D, Glatzel M, Lopera F. Phenotypic profile of early-onset familial Alzheimer's disease caused by presenilin-1 E280A mutation. *JAD* 2012;32:1–12
47. Ranasinghe KG, Kudo K, Hinkley L, et al. Neuronal synchrony abnormalities associated with subclinical epileptiform activity in early-onset Alzheimer's disease. *Brain* 2022;145:744–53
48. Hauser WA, Morris ML, Heston LL, et al. Seizures and myoclonus in patients with Alzheimer's disease. *Neurology* 1986;36:1226–30
49. Vossel KA, Tartaglia MC, Nygaard HB, et al. Epileptic activity in Alzheimer's disease: causes and clinical relevance. *Lancet Neurol* 2017;16:311–22
50. Zhou S, Yu Y. Synaptic E-I balance underlies efficient neural coding. *Front Neurosci* 2018;12:46
51. Barral J, Reyes AD. Synaptic scaling rule preserves excitatory-inhibitory balance and salient neuronal network dynamics. *Nat Neurosci* 2016;19:1690–1696
52. Fu H, Possenti A, Freer R, et al. A tau homeostasis signature is linked with the cellular and regional vulnerability of excitatory neurons to tau pathology. *Nat Neurosci* 2019;22:47–56
53. Fu H, Rodriguez GA, Herman M, et al. Tau pathology induces excitatory neuron loss, grid cell dysfunction, and spatial memory deficits reminiscent of early Alzheimer's disease. *Neuron* 2017;93:533–41 e5
54. Busche MA, Eichhoff G, Adelsberger H, et al. Clusters of hyperactive neurons near amyloid plaques in a mouse model of Alzheimer's disease. *Science* 2008;321:1686–9
55. Palop JJ, Mucke L. Amyloid-beta-induced neuronal dysfunction in Alzheimer's disease: from synapses toward neural networks. *Nat Neurosci* 2010;13:812–8
56. Styr B, Slutsky I. Imbalance between firing homeostasis and synaptic plasticity drives early-phase Alzheimer's disease. *Nat Neurosci* 2018;21:463–73
57. Ingelsson M, Fukumoto H, Newell KL, et al. Early Abeta accumulation and progressive synaptic loss, gliosis, and tangle formation in AD brain. *Neurology* 2004;62:925–31
58. Scheff SW, Price DA, Schmitt FA, et al. Synaptic loss in the inferior temporal gyrus in mild cognitive impairment and Alzheimer's disease. *J Alzheimers Dis* 2011;24:547–57
59. Scheff SW, Price DA. Synapse loss in the temporal lobe in Alzheimer's disease. *Ann Neurol* 1993;33:190–9

60. Scheff SW, Sparks DL, Price DA. Quantitative assessment of synaptic density in the outer molecular layer of the hippocampal dentate gyrus in Alzheimer's disease. *Dementia* 1996;7:226–32
61. DeKosky ST, Scheff SW, Styren SD. Structural correlates of cognition in dementia: quantification and assessment of synapse change. *Neurodegeneration* 1996;5:417–21
62. Scheff SW, DeKosky ST, Price DA. Quantitative assessment of cortical synaptic density in Alzheimer's disease. *Neurobiol Aging* 1990;11:29–37
63. Scheff SW, Price DA. Synaptic density in the inner molecular layer of the hippocampal dentate gyrus in Alzheimer disease. *J Neuropathol Exp Neurol* 1998;57:1146–53
64. Scheff SW, Price DA, Ansari MA, et al. Synaptic change in the posterior cingulate gyrus in the progression of Alzheimer's disease. *J Alzheimers Dis* 2015;43:1073–90
65. Scheff SW, Sparks L, Price DA. Quantitative assessment of synaptic density in the entorhinal cortex in Alzheimer's disease. *Ann Neurol* 1993;34:356–61
66. Scheff SW, Price DA, Schmitt FA, et al. Synapse stability in the precuneus early in the progression of Alzheimer's disease. *J Alzheimers Dis* 2013;35:599–609
67. Bertoldo JB, Muller S, Huttelmaier S. RNA-binding proteins in cancer drug discovery. *Drug Discov Today* 2023;28:103580
68. Julio AR, Backus KM. New approaches to target RNA binding proteins. *Curr Opin Chem Biol* 2021;62:13–23